

A continuous model for sand dunes: Review, new developments and application to barchan dunes and barchan dune fields

Orencio Durán,^{1*} Eric J.R. Parteli² and Hans J. Herrmann^{3,4}

¹ Laboratoire de Physique et Mécanique des Milieux Hétérogènes, (CNRS UMR 7636) ESPCI, 10 rue Vauquelin, 75231 Paris Cedex, France

² Programa de Pós-Graduação em Engenharia Química, Universidade do Ceará, 60455-900, Ceara, Brazil

³ Computational Physics, IfB, HIF E12, ETH Hönggerberg, CH-8093 Zürich, Switzerland

⁴ Departamento de Física, Universidade Federal do Ceará, 60451-970 Fortaleza, Ceará, Brazil

Received 8 October 2008; Revised 8 March 2010; Accepted 1 July 2010

*Correspondence to: O. Durán, Laboratoire de Physique et Mécanique des Milieux Hétérogènes, (CNRS UMR 7636) ESPCI, 10 rue Vauquelin, 75231 Paris Cedex, France. E-mail: orencio.duran@espci.fr

ESPL

Earth Surface Processes and Landforms

ABSTRACT: Basically, sand dunes are patterns resulting from the coupling of hydrodynamic and sediment transport. Once grains move, they modify the surface topography which in turns modifies the flow. This important feedback mechanism lies at the core of continuous dune modelling. Here we present an updated review of such a model for aeolian dunes, including important modifications to improve its predicting power. For instance, we add a more realistic wind model and provide a self-consistent set of parameters independently validated. As an example, we are able to simulate realistic barchan dunes, which are the basic solution of the model in the condition of unidirectional flow and scarce sediments. From the simulation, we extract new relations describing the morphology and dynamics of barchans that compare very well with existing field data. Next, we revisit the problem of the stability of barchan dunes and argue that they are intrinsically unstable bed-forms. Finally, we perform more complex simulations: first, a barchan dune under variable wind strength and, second, barchan dune fields under different boundary conditions. The latter has important implications for the problem of the genesis of barchan dunes. Copyright © 2010 John Wiley & Sons, Ltd.

KEYWORDS: aeolian dunes; hydrodynamic transport; sediment transport

Introduction

The existence of a minimal size for aeolian dunes of about 10–20 m wide has been the main reason behind the many attempts to numerically simulate such bedforms (Werner, 1995; Andreotti *et al.*, 2002a, b; Kroy *et al.*, 2002; Hersen, 2005). In particular, the continuous ‘minimal’ model developed by Sauermaun *et al.* (2001) has been successfully extended to include the full three-dimensional profile of barchan dunes (Schwämmle and Herrmann, 2005), dune collisions (Schwämmle and Herrmann, 2003; Durán *et al.*, 2005), vegetation growth and parabolic dunes (Durán and Herrmann, 2006b), Martian dunes (Parteli and Herrmann, 2007) and, more recently, linear dunes (Parteli *et al.*, 2009) (Figure 1). Since the previous work on the modelling of barchan dunes (Sauermaun *et al.*, 2001; Kroy *et al.*, 2002; Schwämmle and Herrmann, 2005), the ‘minimal’ dune model has experienced several changes. For instance, in the wind model (Durán *et al.*, 2005) with the addition of the non-asymptotic solution for the shear stress perturbation over a smooth hill (Weng *et al.*, 1991), and on the sand transport model with a small set of physical parameters validated using independent transport

data (Durán and Herrmann, 2006a). As we will show, these changes, although small, affect the dune morphology and lead to important consequences in the modelling of dune fields.

Here we present a review of our current version of such a ‘minimal’ model along with new simulations of aeolian barchan dunes (Figure 2). In order to validate the model, we compare the morphology of simulated barchans with measured ones in Morocco (Sauermaun *et al.*, 2000), and we derive relations for the volume, velocity and outflux of barchan dunes, that are consistent with recent measurements (Elbelrhiti *et al.*, 2007). Next, we apply such relations to revisit the stability of an individual barchan dune. Finally, we perform complex simulations of barchan dunes under variable winds, that leads to an instability of the barchan surface, and of barchan dune fields, which highlight the mechanisms behind the genesis of barchan dunes.

Dune Model

The modelling of dunes involves three main stages: (i) a calculation of the wind considering the influence of the

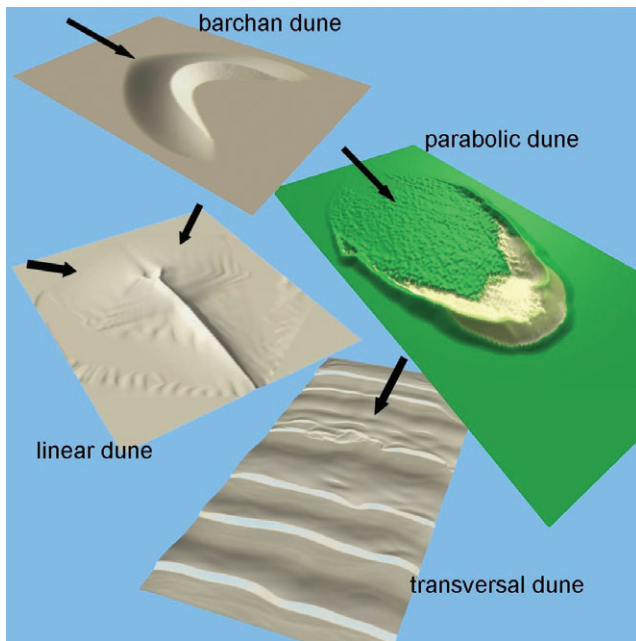


Figure 1. Different types of aeolian dunes simulated with the current ‘minimal’ model. Arrows indicate wind direction. Barchan and transversal dune images are from Durán (2007), the parabolic dune is from Durán and Herrmann (2006b) and the linear dune is from Parteli *et al.* (2009). This figure is available in colour online at wileyonlinelibrary.com

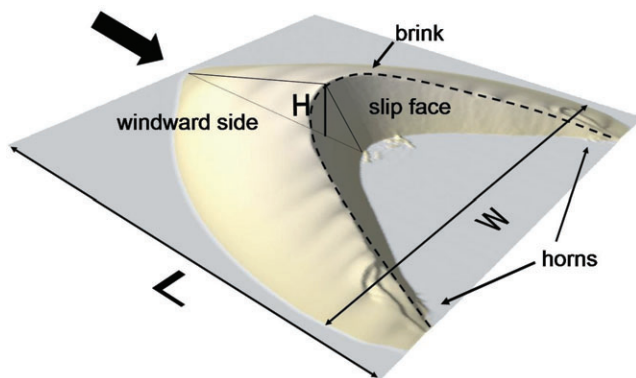


Figure 2. Morphological parameters of a barchan dune (simulated): total length L , height H and width W . Wind direction is indicated by the arrow. Notice the discontinuity in the dune surface, where the brink line separates the slip face (the face where avalanches occurs) from the rest of the dune. This figure is available in colour online at wileyonlinelibrary.com

topography, (ii) a calculation of the sand flux carried by the perturbed wind, and finally (iii) the evolution of the sand surface due to sand erosion, deposition and avalanches. Once the wind starts to blow, it is modified by the surface topography in such a way that it experiences a speed-up on positive slopes and a slowdown on negative ones. The spatial perturbation of the wind velocity leads to an inhomogeneous sand flux that changes the sand surface due to mass conservation. Finally, this topographic change induces a new perturbation on the wind field and the whole cycle repeats.

The coupling of the sand surface evolution and the aeolian sand transport involves two different timescales related, on one hand, to the erosion and deposition processes that change the surface, and, on the other hand, to sand transport and wind flow. A significant change in the sand surface typically needs several hours or even days. In contrast, the time-scale for a

change in the wind flow and the saltation transport is much faster, of the order of seconds. This separation of time-scales leads to an enormous simplification because it decouples the different processes. Therefore, we can use stationary solutions for the wind surface shear velocity u_* and for the resulting sand flux \bar{q} , and later use them for the time evolution of the sand surface $h(x, y)$.

Wind model

The sand transport rate is determined not by the wind velocity, that change with height, but rather by the shear velocity that encodes the friction forces at the surface. This surface shear velocity is sensible to the terrain topography. It is well known that an uphill induces a wind speed-up while a downhill produces a wind slow-down. This effect is crucial for the understanding of dune formation and migration.

We consider a low and smooth relief $h_s(x, y)$, like a hill or a sand dune, which induces a small perturbation $\delta\vec{v}(x, y, z)$ on the wind velocity profile, namely

$$\vec{v}(x, y, z) = \vec{v}_0(z) + \delta\vec{v}(x, y, z). \quad (1)$$

where $\vec{v}_0(z)$ is the unperturbed wind velocity profile of a flat bed.

From the Prandtl turbulent closure, a velocity perturbation leads to a modification of the surface shear stress $\bar{\tau}_0$ over a flat bed given by

$$\bar{\tau}(x, y) = \bar{\tau}_0 + |\bar{\tau}_0| \delta\bar{\tau}(x, y), \quad (2)$$

where $\delta\bar{\tau}(x, y)$ is the shear stress perturbation at the surface $h_s(x, y)$. From now on, subscript ‘0’ means values on a flat bed.

The shear stress perturbation $\delta\bar{\tau}$ is computed according to an analytical work describing the influence of a low and smooth hill on the wind profile and shear stress (Weng *et al.*, 1991). In the Fourier space, this perturbation is proportional to the Fourier transform of the height profile h_s , and depends on the apparent roughness length of the surface, which may include saltation (Durán and Herrmann, 2006a), and on the typical length-scale L of the hill. This length is defined as the mean wavelength of the Fourier representation of the height profile.

By inserting the inverse Fourier transform of the perturbation into Eq. (2), one obtains the modified shear stress, which in terms of the shear velocity reads

$$\vec{u}_*(x, y) = u_*(x, y) \vec{e}_\tau(x, y), \quad (3)$$

where the unity vector $\vec{e}_\tau \equiv \bar{\tau}/|\bar{\tau}|$ defines the actual wind direction and the perturbed shear velocity is

$$u_*(x, y) \approx u_{*0} \sqrt{1 + \delta\tau_x(x, y)}. \quad (4)$$

Here $u_{*0} = \sqrt{\tau_{*0}/\rho}$ denotes the unperturbed shear velocity on a flat bed.

Separation bubble

The formalism for computing the surface wind perturbation does not include nonlinear effects like flow separation and, therefore, it is only valid for smooth surfaces. However, in sand dunes the brink line not only divides the face where avalanches occurs from the rest of the dune, but also, since the repose angle of sand ($\sim 34^\circ$) represents the highest slope in the

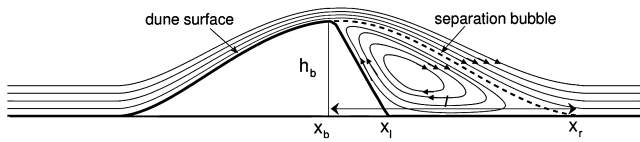


Figure 3. Sketch of the central slice of a barchan dune along with its separation bubble. In the ideal case, the flow separation generates a rotational flow in the region inside the bubble with a negligible sand transport.

dune surface, it establishes a limit at which the wind streamlines separate from the surface (Figure 3). Therefore the above model cannot be used for mature sand dunes with slip faces. One possible solution is to calculate the wind perturbation over an ideal smooth surface $h_s(x, y)$ that comprise the actual profile $h(x, y)$ of the dune and the so-called *separation bubble* $s(x, y)$ (Sauermaun *et al.*, 2001).

The separation bubble is by definition the surface that limits the region of recirculating flow after the brink that results from flow separation (Figure 3). In this region the flow is strongly depressed and thus sand transport can be neglected in a first approximation.

Following the approach of Sauermaun *et al.* (2001), each slice of the surface of the bubble should resemble the separating streamline shape and is modelled by a third-order polynomial in such a way that, for barchans, the region between the horns is inside the bubble (Figure 4(a) and (b)). The coefficients of this polynomial are obtained from

- (i) the continuity of both surfaces at the brink line $x_b(y)$, where $x_b(y)$ is the x -position of the brink for each slice y (Figure 3),
- (ii) the continuity of the first derivatives at the brink, and
- (iii) the smooth conditions $h_s\{x_r(y)\} = 0$ and $h'_s\{x_r(y)\} = 0$ at the re-attachment line $x_r(y)$, where flow re-attaches to the surface again.

The reattachment length $l(y) \equiv x_r(y) - x_b(y)$ for each slice y (Figure 3), is obtained from the assumption that the separation surface has a maximum slope (Sauermaun *et al.*, 2001).

Figure 4a, b show a simulated barchan dune without and with the separation bubble, respectively. The resultant surface $h_s(x, y) \equiv \max\{h(x, y), s(x, y)\}$ is then used to calculate the surface wind shear velocity according to Eqs. (3), as depicted in Figure 4c. The dune topography induces two kind of variations on the wind shear. First, a variation in the strength: at the dune's foot, the wind experiences a slowdown, followed by a speed-up at the windward side and later again a slowdown at dune's horns (see the x -component of the wind, Figure 4d). Second, a variation in wind direction since the wind is forced to surround the dune, as shown in Figure 4e.

Finally, based on the flow separation at the brink, we set the shear velocity to zero inside the separation bubble, i.e. $u_*(x, y) = 0$ for $h(x, y) < h_s(x, y)$.

The corresponding new shear velocity $\bar{u}_*(x, y)$ is used afterwards to calculate the sand transport on the surface $h(x, y)$.

Three-dimensional sand transport model

Characteristic velocity of sand grains

Using the shear velocity, we are able to calculate the modification to the air flow due to the presence of saltating grains. Within the saltation layer, the feedback effect on sand transport results in an effective wind velocity driving the grains (Durán and Herrmann, 2006a). This effective wind velocity v_{eff} can be approximated by the wind velocity $v(x, y, z_1)$ at a reference height z_1 . By assuming as a first approximation no focal point

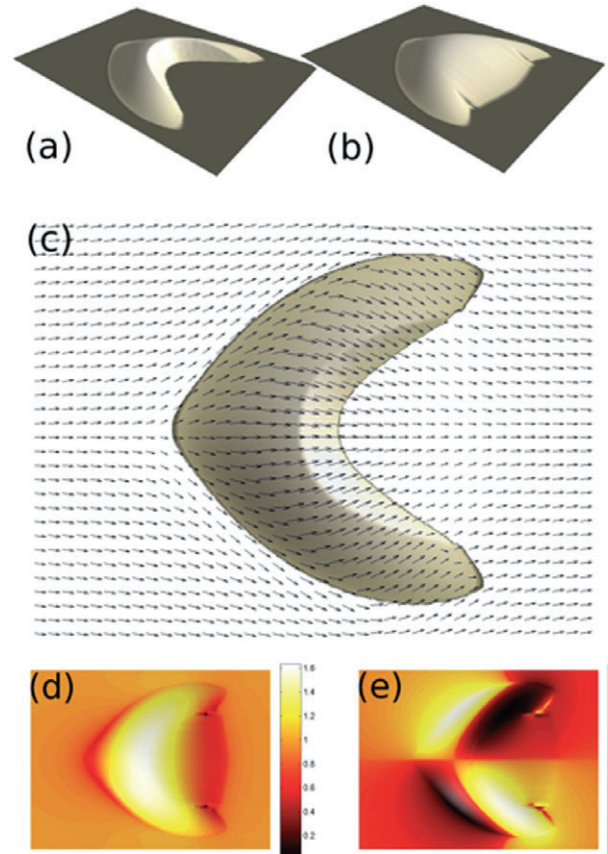


Figure 4. Simulated barchan dune (a) and its separation bubble (b). The normalized wind shear velocity \bar{u}_*/u_{*0} (Eq. 3) over a barchan dune including the separation bubble (b), is plotted in (c). Note that u_* is proportional to the wind velocity field at a fixed height from the dune surface. Both components u_{*x} and u_{*y} are included in (d) and (e) for comparison. This figure is available in colour online at wileyonlinelibrary.com

on the velocity profile, and taking into account the characteristic height of the saltation layer $z_m \sim 20$ mm, the grain-based roughness length $z_0 \sim 10$ μm and the reference height $z_1 \sim 3$ mm, the effective wind velocity can be approximated as (Durán and Herrmann, 2006a)

$$v_{\text{eff}}(x, y) \approx \frac{u_{*t}}{\kappa} \left[\ln \frac{z_1}{z_0} + \frac{z_1}{z_m} \left\{ \frac{u_*(x, y)}{u_{*t}} - 1 \right\} \right], \quad (5)$$

where u_{*t} is the shear velocity threshold for sand transport.

The collective motion of sand grains in the saltation layer is characterized by their horizontal velocity u_s at the reference height z_1 . For simplicity, we call it 'sand grain velocity' even if it is referred to the total horizontal motion of the grains and not to individual grains. In the saturated state, this velocity is determined from the momentum balance between the drag force acting on the grains, the loss of momentum when they splash on the ground, and the downhill gravity force (Sauermaun *et al.*, 2001; Kroy *et al.*, 2002):

$$\frac{(\bar{v}_{\text{eff}} - \bar{u}_s)|\bar{v}_{\text{eff}} - \bar{u}_s|}{u_f^2} - \frac{\bar{u}_s}{2\alpha|\bar{u}_s|} - \bar{\nabla}h = 0, \quad (6)$$

where $\bar{v}_{\text{eff}} \equiv v_{\text{eff}}\bar{e}_\tau$ and u_f is the grain settling velocity.

For steep surfaces Eq. (6) must be solved numerically. However, since the local slope for dunes cannot exceed the

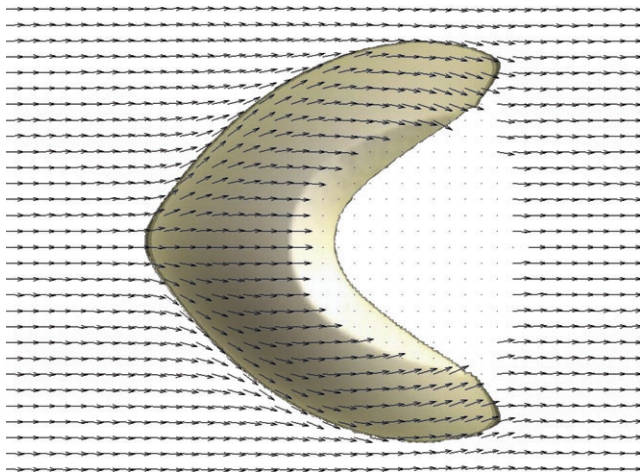


Figure 5. Vector diagram of the normalized characteristic sand grains velocity \bar{u}_s/u_{s0} over a barchan dune. The normalization constant is defined as $u_{s0} \equiv u_s(u_{*0})$ and represents the sand velocity on a flat bed. This figure is available in colour online at wileyonlinelibrary.com

repose angle of sand ($\approx 34^\circ$), we assume the direction of the sediment transport, given by $\bar{u}_s/|\bar{u}_s|$, is co-linear to the wind direction \bar{e}_τ in the second term of Eq. (6). In this case, the velocity of sand grains can be approximated by

$$\bar{u}_s \approx \left(v_{\text{eff}} - \frac{u_t}{\sqrt{2\alpha A}} \right) \bar{e}_\tau - \frac{\sqrt{2\alpha} u_t}{A} \bar{\nabla} h, \quad (7)$$

where $A \equiv |\bar{e}_\tau + 2\alpha \bar{\nabla} h|$. From this equation, the sand velocity in the saturated state has two terms. The first one points toward the wind direction, while the second one is directed along the surface gradient. Both terms account for the competing effects of wind and gravity on the motion of sand grains. Figure 5 shows the characteristic horizontal velocity of sand grains over a barchan dune. Note the strong deviation of the sand flux at the dune's base and the 'trap' effect of the slip face due to flow separation at the brink. The trapped grains accumulate on the top of the slip face before falling down in avalanches.

Saltation flux

From Eq. (6) we can obtain the saturated sand flux q_s over an irregular sand surface $h(x, y)$. However, how does the sand flux evolve toward the saturated state from a given initial or boundary value?

On the one hand, the saltation sand flux over a sand bed increases due to the cascade of splashed grains that enter the flow, while, on the other hand, it cannot grow without limit due to the momentum reduction the grain motion exerts on the wind. In this context, Sauermaun *et al.* (2001) proposed a nonlinear transport equation that describes the spatial evolution of the saltation sand flux $q \equiv |\bar{q}|$:

$$\nabla \cdot \bar{q} = \frac{q}{l_s} \left(1 - \frac{q}{q_s} \right) \begin{cases} \Theta(h) & q < q_s \\ 1 & q \geq q_s \end{cases}, \quad (8)$$

where $q_s \equiv |\bar{q}_s|$ is the saturated sand flux and l_s is the length that characterizes the relaxation toward saturation, also called 'saturation length'. From Eq. (8) the sand flux grows exponentially at small values of q , with the characteristic length l_s , while, close to the maximum flux q_s , the second term $1 - q/q_s$ leads to saturation. The symbol $\Theta(x)$ represents the Heaviside

function (equal to 1 for positive x and 0 otherwise), and guarantees that if there is no sand available ($h = 0$) an under-saturated sand flux $q < q_s$ cannot increase.

The saturated sand flux and the saturation length are given by

$$\bar{q}_s(u_*) = \frac{2\alpha}{g} \frac{\rho}{\rho_{\text{sand}}} (u_*^2 - u_{*t}^2) \bar{u}_s, \quad (9)$$

$$l_s(u_*) = \frac{2\alpha |\bar{u}_s|^2}{\gamma g} \frac{1}{(u_*/u_{*t})^2 - 1}, \quad (10)$$

where α is an effective restitution coefficient (Durán and Herrmann, 2006a) and γ is a model parameter accounting for the splash process (Sauermaun *et al.*, 2001). From now on we will denote the saturated flux over a flat bed as $Q \equiv q_s(u_{*0})$.

Figure 6 depicts the normalized saltation sand flux q/Q over a barchan dune that results from solving Eq. (8) with an imposed boundary condition. In this case we impose a small influx $q_{\text{in}} = 0.1Q$. In the figure, the barchan dune is surrounded by a flat rocky surface. Therefore, the sand flux remains constant until it reaches the sand surface. Afterwards, the flux evolves following in general lines the changes of the wind shear velocity u_* (Figure 4) i.e. the flux increases on the windward side of the dune and decreases at the dune's horns, while in the region inside the separation bubble (the slip face and between the horns) there is no sand motion and thus no sand flux.

This transport model, that can be labelled as complex, contrasts with more simplified approaches, for instance that of Hersen (2005), where a constant value is set for l_s and a linear order development for the saturated flux in terms of the perturbed shear. Although the basic elements for obtaining the main instabilities are rather simple, we have checked that, in order to get realistic dunes, all the complexity has to be included.

The time evolution of the surface

The spatial change of the sand flux showed in Figure 6 and described by the sand transport equation (8) defines the temporal change of the sand profile $h(x, y)$. According to the mass conservation

$$\frac{\partial h}{\partial t} = -\nabla \cdot \bar{q}. \quad (11)$$

Following Eq. (8), wherever the sand flux is below saturation ($q < q_s$) the amount of sand transported by the wind increases and erosion takes place ($\partial h/\partial t < 0$). Otherwise, in case of over-saturation ($q > q_s$), the amount of sand carried by the wind is beyond its limits and deposition occurs ($\partial h/\partial t > 0$).

Figure 7 shows the sand erosion-deposition pattern over a barchan dune. The dune is clearly divided into two parts: the windward side, where erosion takes place, and the lee side, comprising the slip face and the horns, where sand is deposited. Furthermore, through the erosion-deposition process given by Eq. (11), the dunes are by definition not static but dynamical objects. They are essentially sculpted by the wind, which takes sand from one place to the other following certain rules. This explains how a millimetre-scaled process like the sand transport by grain saltation can produce large structures like dunes. It is not the transport mechanisms but the wind field in its interdependence with the surface topography, which drives the dune's formation and evolution.

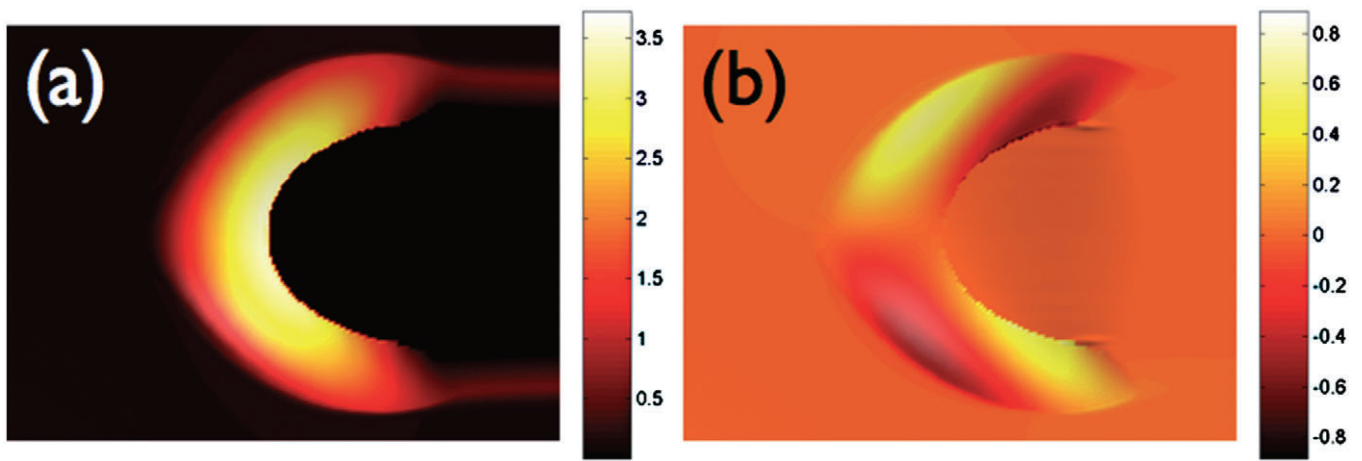


Figure 6. (a) Parallel component, along-wind direction, and (b) transverse component of the normalized saltation sand flux q/Q over a barchan dune as resulting from the wind field depicted in Figure 4. The wind blows from left to right carrying a normalized influx equal to 0.1. The parallel component of the flux is clearly higher than the transverse component, even if the later is not negligible. This figure is available in colour online at wileyonlinelibrary.com

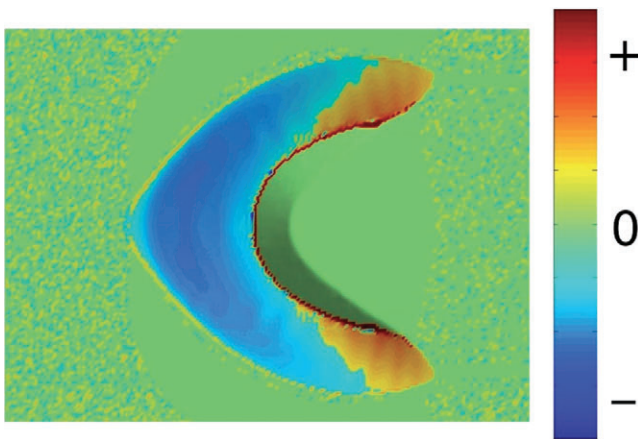


Figure 7. Sand erosion (–) and deposition (+) pattern on a barchan dune. Note that sand is eroded from the dune's windward side while it is trapped by the slip face or deposited on the horns. This figure is available in colour online at wileyonlinelibrary.com

Avalanches

The evolution of a sandy surface is determined, as was previously shown, by the aeolian erosion-deposition process, as a consequence of the spatial inhomogeneity of the sand flux over a wavy surface. However, in the slip face inside the separation bubble, there is no sand transport, and sand grains accumulate there after crossing the brink. In this region non-aeolian mechanisms of sand transport take place, namely sand avalanches.

Taking into account that the characteristic time of avalanche events is orders of magnitude smaller than the characteristic time involved in the whole surface evolution, we consider an effective model that instantaneously relaxes the gradient of the sand surface toward the sand repose angle. If the slope of the surface exceeds the static angle of repose, sand is redistributed according to the sand flux:

$$\bar{q}_{\text{aval}} = E \{ \tanh(|\nabla h|) - \tanh(\tan \theta_{\text{dyn}}) \} \frac{\nabla h}{|\nabla h|}. \quad (12)$$

By using this flux, the surface is relaxed according to Eq. (11), until the maximum slope lies below the dynamic angle of

repose, θ_{dyn} . We include the hyperbolic tangent function to improve convergence.

Model parameters

Wind model

The wind model has only two parameters, the apparent roughness length and the shear velocity u_{*0} over a flat bed. The first one is fixed to the value 1 mm, which coincides with the peak value of the roughness length curve in Durán and Herrmann (2006a) for the characteristic grain diameter in sand dunes $d \approx 0.25$ mm. The unperturbed shear velocity u_{*0} is defined by the initial condition.

Separation bubble model

The model for the separation bubble only has one parameter, the maximum slope allowed for the separation surface, which is fixed to the value 0.2, smaller than the value assigned by Sauermann (0.25) corresponding to a maximum angle of 14° (Sauermann *et al.*, 2001). We select 0.2 after performing calculations of the wind profiles over real Moroccan dunes (unpublished).

Sand transport model

The sand transport model has five parameters. Four of them, z_0 , z_m , z_1 and α , are not free parameters and were obtained and validated in Durán and Herrmann (2006a) in terms of the grain density $\rho_g \approx 2650$ kg m⁻³, grain diameter $d \approx 0.25$ mm, air density $\rho_i \approx 1.225$ kg m⁻³, air kinematic viscosity $\nu \approx 1.5 \times 10^{-5}$ m² s⁻¹, gravity acceleration $g \approx 9.8$ m s⁻² and drag coefficient C_d . The remaining parameter is $\gamma \approx 0.2$ and describes the efficiency of the splash process to submit grains into the flow (Sauermann *et al.*, 2001).

Avalanche model

The only free parameter in the model for avalanches is E which has dimension of flux. After some test of convergence we select the value $E = 0.9$ kg m⁻¹ s⁻¹. Of course, since the avalanches are modelled just as a slope relaxation, the value of E has no physical meaning. The other two parameters are the static $\theta_{\text{stat}} \approx 34^\circ$ and dynamic angle of repose $\theta_{\text{dyn}} \approx 33^\circ$ for sand.

Barchan Dune Simulations

In this section we study barchan dunes using numerical simulations (Figure 8) and present some new scaling relations

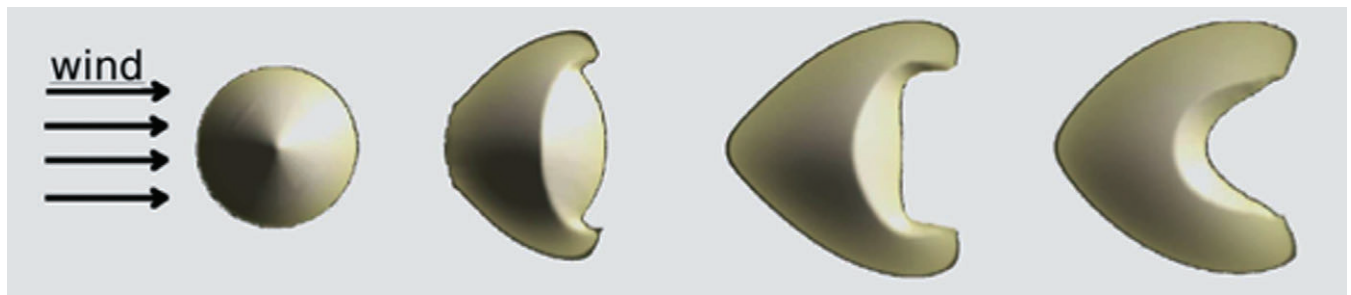


Figure 8. Simulation of the formation of a 6 m high barchan dune from an initial sand pile after the equivalent of ~ 1 year of constant wind blow. This figure is available in colour online at wileyonlinelibrary.com

between the barchan volume, velocity and flux balance with their size. Comparing these scaling laws with measured data, we validate the predictions of our dune model including an improved sand transport model and the corresponding parameters (Durán and Herrmann, 2006a).

Barchans are isolated sand dunes that emerge when wind is uni-directional and sand is sparse (Figure 2). Under these conditions, the barchan shape represents the equilibrium shape toward which any initial sand surface over a non-erodible substrate evolves. They arise from the numerical integration of Eqs. (3), (8) and (11) for a given initial surface, an unperturbed shear velocity u_{*0} , oriented along the x -direction, and a constant influx q_{in} at the input boundary $x = 0$. Since u_{*0} unequivocally defines the maximum sand flux Q over a flat bed, we can use either u_{*0} or Q to characterize the unperturbed wind.

Therefore, the simulations only have two free parameters, the sand supply, encoded in q_{in} , and the wind strength, encoded in u_{*0} or $Q(u_{*0})$.

Figure 8 depicts the evolution of the profile $h(x, y)$ of a sand pile towards a barchan dune, while Figure 9 compares the three-dimensional characteristic 'C' shape of the simulated and a measured Moroccan barchan (Sauermaun *et al.*, 2000). Both dunes are very similar except in the horns. This typical simulation was performed using zero influx $q_{in} = 0$ and a flat bed shear velocity $u_{*0} = 0.4 \text{ m s}^{-1}$, a realistic value for dune fields.

Morphologic relationships

The morphology of a barchan dune is characterized by well-known linear scalings between the dune's width W , total length L , windward side length L_w , mean horns length L_{horn} and the dune's height H (Finkel, 1959; Long and Sharp, 1964; Hastenrath, 1967; Sauermaun *et al.*, 2000; Elbelrhiti *et al.*, 2007). Furthermore, it is also known that the dune size scales with the only characteristic length of the model: the saturation length l_s proportional to the characteristic length of the flow drag, $l_{drag} = d\rho_g/\rho_f$, where d is the grain diameter and ρ_g/ρ_f is the grain to flow density ratio.

Figure 10 shows one of these scalings, the width-height relationship, where both dune height and width are rescaled by l_{drag} in order to include data from underwater dunes (Hersen *et al.*, 2002). The width-height relationship has the form $W/l_{drag} = a_w H/l_{drag} + b_w$, and thus the barchan shape is only scale invariant for large sizes, i.e. the ratio $H/W = H/(a_w H + b_w l_{drag})$ tends to the constant $1/a_w$ at large H . However, for small sizes, $H/l_{drag} < 5 b_w/a_w \sim 3$, the barchan shape is size-dependent. This rupture of the scale invariance at small sizes is a consequence of the saturation length $l_s \propto l_{drag}$ given in Eq. (9) which also determines the minimal size for barchan dunes (Kroy *et al.*, 2002; Andreotti *et al.*, 2002b).

Simulations for different wind strength and influx show that the barchan volume V scales as w^3 with a proportionality

factor c that is independent of both the sand flux over a flat bed Q and the influx q_{in} . The value $c \approx 0.017$ is obtained from the fit in Figure 10. This simple scaling was also recently found in field measurements (Hersen *et al.*, 2004; Elbelrhiti *et al.*, 2007).

Velocity

Since the pioneer work of Bagnold (1941), it is also well-known that the barchan velocity v scales with the inverse of its size and is proportional to the saturated flux Q on a flat bed. However, although the relationship between v with Q is well established, there is still a debate about which size should be used. Bagnold (1941) showed, through a simple mass conservation analysis, that v scales with the inverse of the dune's height, namely $v \propto 1/H$. Alternatively, other authors propose a scaling with the dune's length (Sauermaun *et al.*, 2001; Schwämmle and Herrmann, 2005), or a more complex relation of the type $v \propto 1/(H + H_0)$ to fit dune measurements (Andreotti *et al.*, 2002a,b; Hersen *et al.*, 2004; Elbelrhiti *et al.*, 2005).

Using simulated barchans, we find that the velocity v scales with the inverse of their width w , as shown in Figure 11. Therefore, we consider

$$v \approx \alpha \frac{Q}{W}, \quad (13)$$

with the constant $\alpha \approx 50$ in very good agreement with previous studies (Hersen, 2005).

Stability: Flux balance in a barchan dune

From the dynamical point of view, the stability of barchan dunes is a particular important question. Based on previous simulations, it has been predicted that barchan dunes are unstable (Sauermaun *et al.*, 2001; Hersen *et al.*, 2004).

In order to illustrate the dune size instability, we analyze the flux balance equation. A barchan dune can be seen as an object that captures some amount of sand from the windward side and releases another amount from the horns while trapping a fraction of it at the slip face (Figure 6). Therefore, the flux balance in a dune is given by the difference between the net influx Q_{in} and the net outflux Q_{out} . Since both scale with the product WQ , the volume conservation reads

$$\frac{dV}{dt} = Q_{in} - Q_{out} = WQ \left(\frac{q_{in}}{Q} - \frac{q_{out}}{Q} \right), \quad (14)$$

where q_{in} and q_{out} are the dune influx and outflux per unit length, respectively, and V is the volume of the dune.

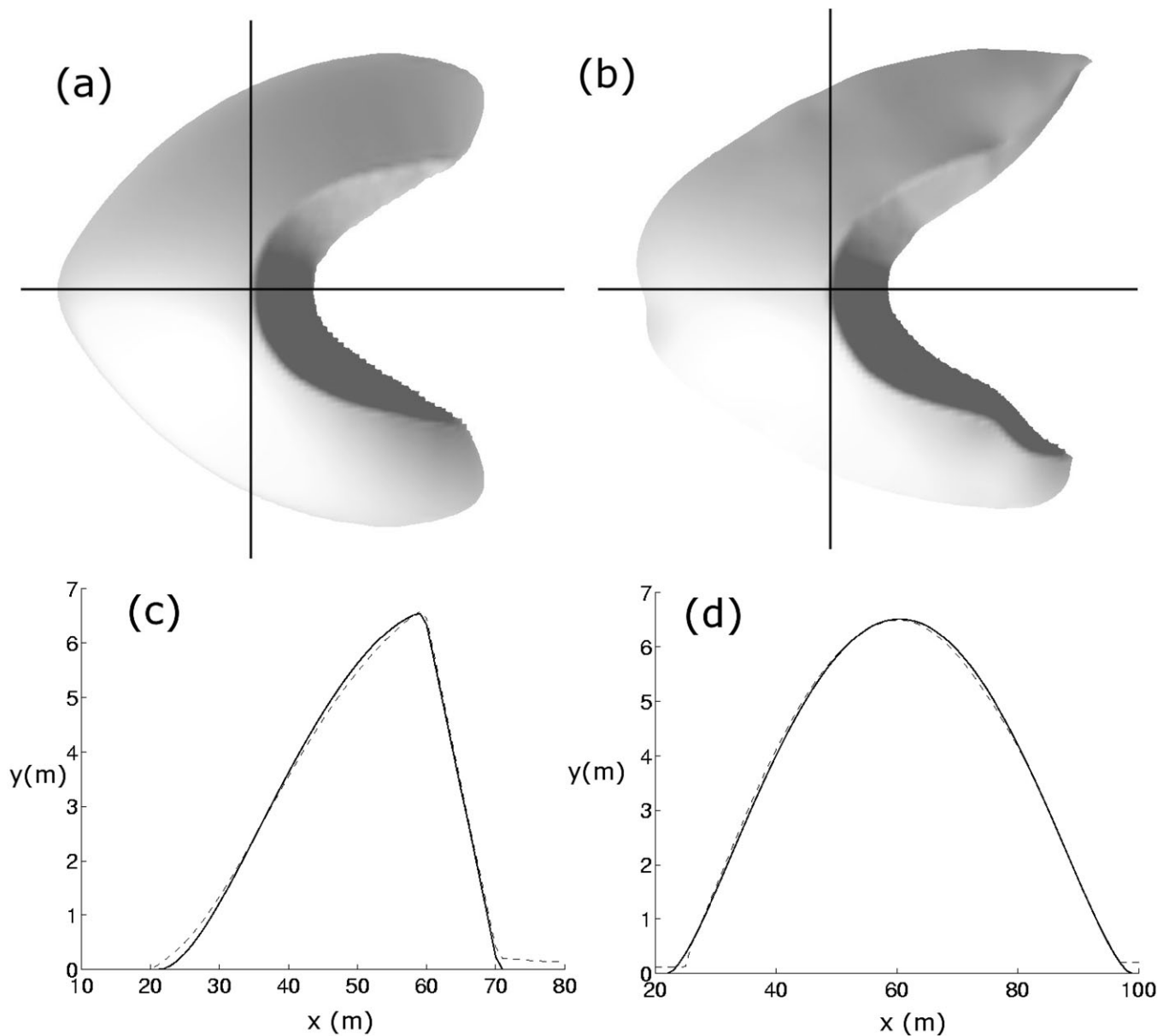


Figure 9. Comparison between a 6 m high (a) simulated and (b) measured barchan. (c) and (d) respectively show the longitudinal and transversal central slices of both the simulated (full line) and the measured (dashed line) dune. Both dunes have the same scale.

Measurements on single simulated barchans with a constant influx show that, for small widths $W < W_c$, the outflux is saturated which means that the dune does not have a slip face anymore, i.e. it becomes a dome. However, for higher width the outflux relaxes as $1/W^2$ to a constant value that scales linearly with the influx with a slope smaller than 1 (Figure 12), namely

$$\frac{q_{out}}{Q} = a \frac{q_{in}}{Q} + b + \left(\frac{W_c}{W}\right)^2, \quad (15)$$

where $a \approx 0.45$, $b \approx 0.1$ and W_c are fit parameters. Therefore, at large sizes, there are two different regimes: for $q_{in} < 0.18Q$ the outflux is higher than the influx and the dune shrinks, while for $q_{in} > 0.18Q$ the influx overcomes the outflux and the dune grows (Figure 12, inset). The dimensionless barchan outflux q_{out}/Q is proportional to the total horns width fraction $2W_{horn}/W$, where W_{horn} denotes the width of one horn (Figure 2). Thus, the flux balance on a barchan dune is determined by its morphology.

The deviation from the scale invariance in the dune outflux q_{out} is expressed by the last term of Eq. (15), which is a

consequence of the non-scale invariance for small dunes. However, since the critical width $W_c \sim 20 l_{drag}$ is of the order of the minimal dune width, the nonlinear term is very small and can be neglected. Therefore, we can consider to a first approximation dune horns as scale invariant, in agreement with measurements on barchan dunes in south Morocco and in the Arequipa region, Peru (Elbelrhiti *et al.*, 2007). Notice that in the scale-invariant regime, the dune instability arises due to the relation between the outflux and the influx (Figure 12, inset), and does not depend on the dune size, a different argument from that of Hersen *et al.* (2004) where dune influx did not play any role in dune morphology.

After combining Eqs. (14), (15) and the volume scaling $V = cW^3$, the mass balance becomes

$$\frac{dW}{dt} = \frac{(1-a)Q}{3cW} \left(\frac{q_{in}}{Q} - \frac{q_c}{Q} \right), \quad (16)$$

where $q_c = bQ/(1-a) \approx 0.18Q$ denotes the equilibrium influx at which the dune volume does not change. However, this

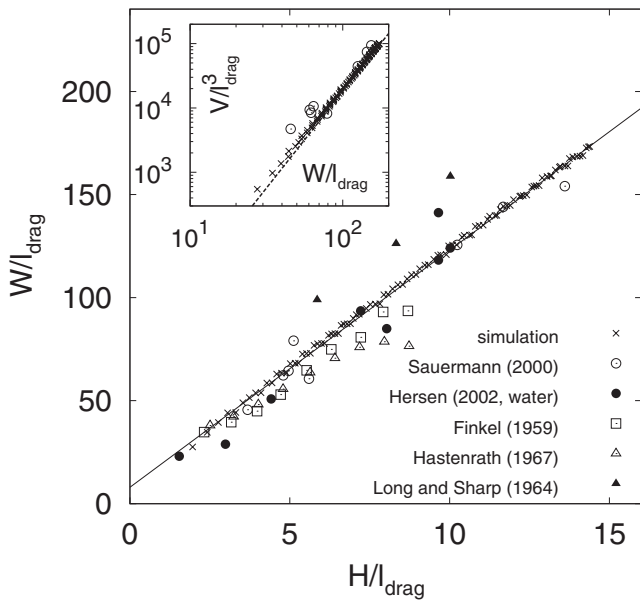


Figure 10. Height H and width W relationship for simulated and measured barchan dunes (including some data underwater) with the linear regression $W = 12H + 8l_{drag}$. Inset: Cubic scaling of the volume of simulated barchan dunes with their width. The volume data of measured Moroccan dunes are included for comparison.

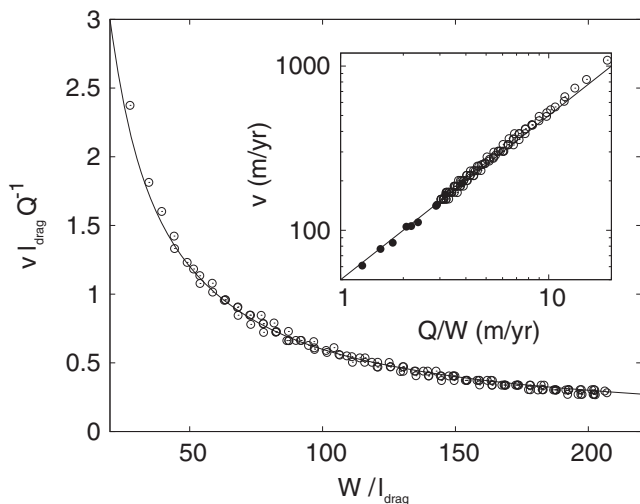


Figure 11. The dimensionless velocity $v_{l_{drag}}/Q$ of simulated barchan dunes (symbols) scaled as l_{drag}/W (full line) for a constant saturated flux Q . Inset: barchan dune velocity as a function of the ratio Q/W for different values of Q .

equilibrium is unstable since there are no mechanisms by which barchan dunes can change their outflux to adjust it to a given influx.

Towards More Complex Patterns

In sharp contrast to the results presented so far, real dunes are subjected to variable winds (both in strength and direction) and they arise in large groups, called dunes fields, where they interact in a complex way (Elbelrhiti *et al.*, 2005).

In order to approach such conditions, we have performed simulations of the evolution of barchan dunes under a unidirectional wind with a variable strength, and simulations of barchan dune fields under a constant wind and with two different boundary conditions.

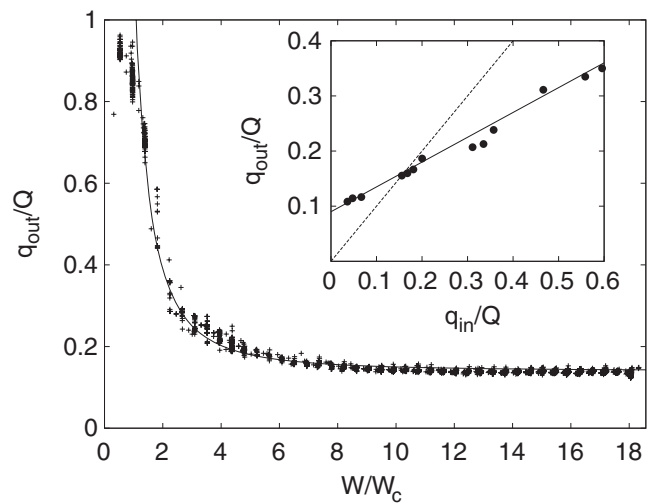


Figure 12. Relation between the dune outflux and the dune width W . The solid line represent the scaling with $1/W^2$ given in the text. Inset: the dune outflux as a linear function of the dune influx (solid line) with a slope smaller than 1 (dashed line).

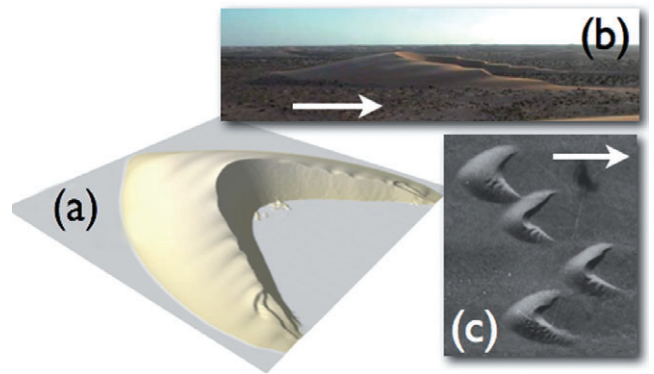


Figure 13. (a) Simulated mature barchan dune under a variable strength wind. (b) and (c) are real examples for comparison. This figure is available in colour online at wileyonlinelibrary.com

Variable wind strength

Mimicking seasonal winds, we impose on a large (10 m high) sand heap a variable wind shear velocity, which fluctuates from $0.5u_{*t}$ to $5u_{*t}$, based on real data from Pecem, on the northeastern Brazilian coast.

Following the dune evolution, the resulting barchan shape has new highly realistic morphological features, in particular sharper horns and, more importantly, instabilities at the windward side (Figure 13). These instabilities result from the dependence of the saturation length with the wind shear velocity, which predicts a smaller characteristic dune length for large winds. Therefore, in the windy season, the already stabilized dune surface becomes unstable for the new characteristic length, with surface waves that leave through the dune horns, in a very similar way to those recently observed on real fields (Elbelrhiti *et al.*, 2005). We have also observed a similar effect by changing wind direction instead of wind strength. In this case, the horns becomes unstable for large wind angles.

Barchan dune fields

Using continuous transport models, barchan dunes have been nucleated individually only from an existing large pile or heap

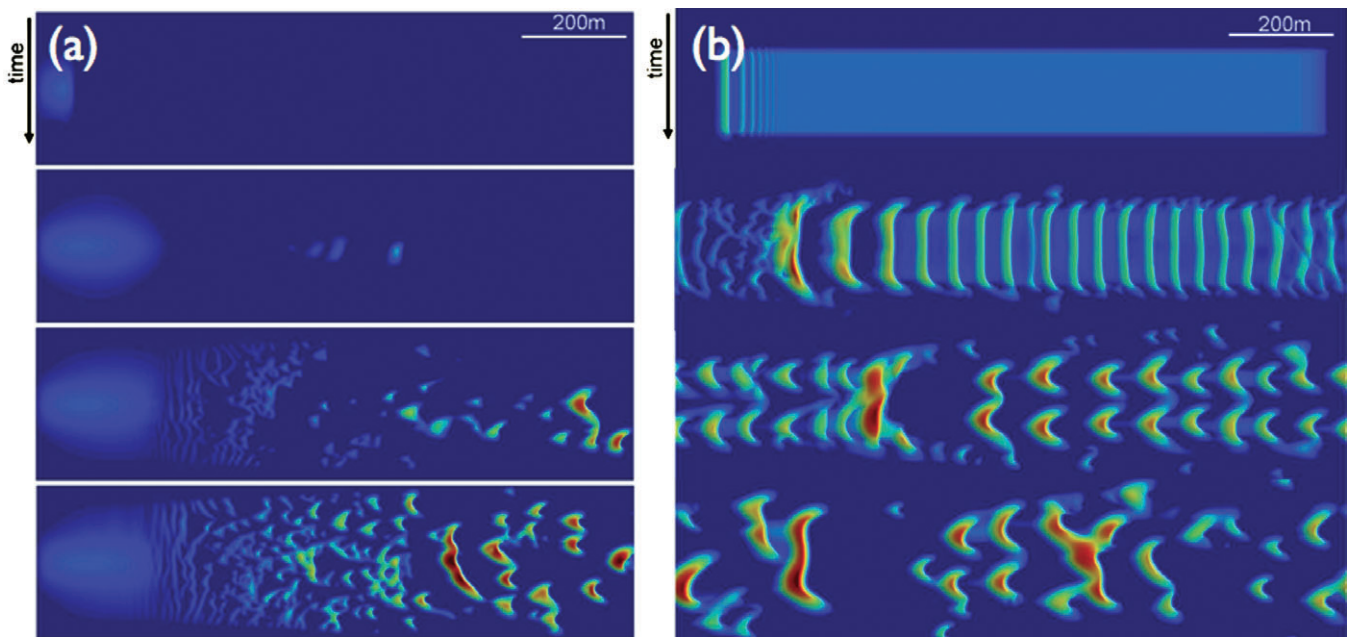


Figure 14. (a) Barchan dune field emerging from an open boundary 'beach' condition. (b) Barchan field from an initial flat sand bed under periodic boundaries. In both cases, wind blows from left to right. Dune height is denoted by the colour scale: from dark blue (flat non-erodible surface) to red (~ 6 m). This figure is available in colour online at wileyonlinelibrary.com

of sediment. However, in the field the picture is rather different, with barchans emerging in large groups from coastal zones or from more complex larger dunes. In this context, there are several important questions regarding the size selection of dunes and the nucleation of barchans.

As a first attempt to simulate a real barchan field, we performed large-scale simulations using two boundary conditions: first, an initial very small hill (~ 1 m height) over a non-erodible surface, was placed at the incoming boundary and subjected to a saturated influx (mimicking a sandy beach, Figure 14a). Since the influx is maximum, the hill cannot be eroded and, instead, it grows until it becomes unstable, continuously producing transversal dunes. Once these dunes propagate over the non-erodible surface, they become unstable and split into barchans. This simple mechanism leads to realistic barchan dune fields as shown in Figure 14a.

Second, an initial flat bed placed at the centre of the field was subjected to a unidirectional flow under periodic boundaries. In this case, the flat bed destabilizes into transversal dunes that in turn split into barchans, leading first to a regular pattern that becomes disordered once dunes collide with each other. Within this picture of dunes colliding and exchanging sand flux, there is apparently a dune size selection process, however any statistical analysis is difficult due to the cost of such calculations.

Conclusions

We have presented the current version of a 'minimal' dune model, which has been the core of several bedform simulations, ranging from parabolic to linear dunes. The model was qualitatively validated by comparing some characteristic parameters of simulated barchan dunes with empirical data. Next, we studied the stability of barchan dunes, showing that they are intrinsically unstable not only due to their scale invariance, as has been shown by other authors, but also because the influx is able to change the dune morphology, in particular the relative width of the horns.

Finally, we have shown that the continuous dune model is able to reproduce real morphological features, like the surface instability analyzed by Elbelrhiti *et al.* (2005) and also to produce actual dune fields. This opens the way to the study of barchans under real conditions, addressing several open problems from the size selection of dunes to the genesis of barchans and more complex patterns.

Although this continuous dune model correctly describes the main aspects of the barchan morphology and dynamics, we would like to stress that it is far from being perfect. For instance, the separation bubble neglects the secondary sediment transport in the slip face and between the horns, the saturation length does not include the inertia of sand grains and thus it fails at large winds, and the dependence of the shear stress threshold with the local slope is neglected (Andreotti and Claudin, 2007; Parteli *et al.*, 2007).

References

- Andreotti B, Claudin P, Douady S. 2002a. Selection of dune shapes and velocities. Part 1: Dynamics of sand, wind and barchans. *European Physical Journal B* **28**: 315–319.
- Andreotti B, Claudin P, Douady S. 2002b. Selection of dune shapes and velocities. Part 2: A two-dimensional modeling. *European Physical Journal B* **28**: 321–339.
- Andreotti B, Claudin P. 2007. Comment on "Minimal size of a barchan dune". *Physical Review E* **76**: 066301.
- Bagnold RA. 1941. *The physics of blown sand and desert dunes*. Methuen: London.
- Durán O. 2007. 'Vegetated dunes and barchan dune fields'. PhD thesis, University of Stuttgart.
- Durán O, Herrmann HJ. 2006a. Modelling of saturated sand flux. *Journal of Statistical Mechanics* P07011.
- Durán O, Herrmann HJ. 2006b. Vegetation against dune mobility. *Physical Review Letters* **97**: 188001.
- Durán O, Schwämmle V, Herrmann HJ. 2005. Breeding and solitary wave behavior of dunes. *Physical Review E* **72**: 021308.
- Elbelrhiti H, Claudin P, Andreotti B. 2005. Field evidence for surface-wave-induced instability of sand dunes. *Nature* **437**: 720.
- Elbelrhiti H, Andreotti B, Claudin P. 2007. Barchan dune corridors: Field characterization and investigation of control parameters.

- Journal of Geophysical Research* **113**: F02S15. DOI: 10.1029/2007JF000767.
- Finkel HJ. 1959. The barchans of southern Peru. *Journal of Geology* **67**: 614–647.
- Hastenrath S. 1967. The barchans of the Arequipa region, southern Peru. *Zeitschrift für Geomorphologie* **11**: 300–331.
- Hersen P. 2005. Flow effects on the morphology and dynamics of aeolian and subaqueous barchan dunes. *Journal of Geophysical Research* **110**: F04S07.
- Hersen P, Douady S, Andreotti B. 2002. Relevant length scale of barchan dunes. *Physical Review Letters* **89**: 264–301.
- Hersen P, Andersen KH, Elbelrhiti H, Andreotti B, Claudin P, Douady S. 2004. Corridors of barchan dunes: stability and size selection. *Physical Review E* **69**: 011304.
- Kroy K, Sauermann G, Herrmann HJ. 2002. Minimal model for sand dunes. *Physical Review Letters* **68**: 54301.
- Long JT, Sharp RP. 1964. Barchan-dune movement in Imperial Valley. *Geological Society of America Bulletin* **75**: 149–156.
- Parteli EJR, Herrmann HJ. 2007. Saltation transport on Mars. *Physical Review Letters* **98**: 198001.
- Parteli EJR, Durán O, Herrmann HJ. 2007. Reply to ‘Comment on “Minimal size of a barchan dune”’. *Physical Review E* **76**: 063302.
- Parteli EJR, Durán O, Tsoar H, Schwämmle V, Herrmann HJ. 2009. Dune formation under bimodal winds. *Proceedings of the National Academy of Science* **106**: (52) 22085–22089.
- Sauermann G, Rognon P, Poliakov A, Herrmann HJ. 2000. The shape of the barchan dunes of southern Morocco. *Geomorphology* **36**: 47–62.
- Sauermann G, Kroy K, Herrmann HJ. 2001. A continuum saltation model for sand dunes. *Physical Review E* **64**: 31305.
- Schwämmle V, Herrmann HJ. 2003. Solitary wave behaviour of dunes. *Nature* **426**: 619.
- Schwämmle V, Herrmann HJ. 2005. A model of barchan dunes including lateral shear stress. *European Physical Journal E* **16**: 57–65.
- Weng WS, Hunt JCR, Carruthers DJ, Warren A, Wiggs GFS, Livingstone I, Castro I. 1991. Air flow and sand transport over sand dunes. *Acta Mechanica (Suppl.)* **2**: 1–22.
- Werner BT. 1995. Eolian dunes: Computer simulations and attractor interpretations. *Geology* **23**: 1107–1110.